Physica Medica 60 (2019) 66–75

Contents lists available at ScienceDirect

Physica Medica

journal homepage: www.elsevier.com/locate/ejmp

Original paper

Geant4 physics list comparison for the simulation of phase-contrast mammography (XPulse project)

V. Beaudoux[a,*], G. Blin[a], B. Barbrel[b], G. Kantor[c], C. Zacharatou[c]

[a] Bordeaux University, LaBRI, CNRS UMR 5800, F-33400 Talence, France
[b] ALPhANOV Optics and Lasers Technology Center, Bordeaux, France
[c] Department of Radiotherapy, Institut Bergonié, Comprehensive Cancer Center, 229 cours de l'Argonne, 33076 Bordeaux, France

ARTICLE INFO

Keywords:
Geant4
Mammography
Monte Carlo

ABSTRACT

Purpose: Breast cancer is the most frequent cancer in women. Early and accurate detection of the disease is a major factor in patient survival. To this end, phase-contrast imaging has gained significant interest in recent years. The aim of this work was to validate the physics models of a Geant4 mammography imaging simulation (in the context of the XPulse project) by comparing to EGSnrc results.

Methods: We used three Geant4 electromagnetic physics lists of the version 10.4 of the toolkit: Standard, Livermore and Penelope. We calculated energy distributions in homogeneous and inhomogeneous phantoms and breast doses in DICOM images. The simulations used photon beams of energies 20–100 keV. The Geant4 calculations were compared with EGSnrc/DOSXYZnrc simulations.

Results: We found a very good agreement between the Standard Electromagnetic option 4 and Livermore Physics Lists (within 1% for all beam energies). Larger differences were found between Standard Electromagnetic option 4 and Penelope Physics Lists (about 4%). The agreement of longitudinal energy distributions between Geant4 Standard Electromagnetic option 4 and EGSnrc was good in water and light biological materials, but important discrepancies were found in heavy elements. We confirmed with both codes that dose to the breast is minimal at beam energy around 60 keV.

Conclusions: Overall, we found good agreement between the option 4 of the Standard Electromagnetic physics list and Livermore physics lists of Geant4, as well as EGSnrc for materials relevant to mammography screening. Further investigations are needed for the case of heavier materials.

1. Introduction

Breast cancer is the most frequent form of cancer in women. The implementation of mammography systems and organised breast screening has allowed for a better control of the disease since the 1970s due to early detection of the disease. Currently, the reference technology for breast cancer screening is digital mammography. The dose deposited in breast tissue during a diagnostic procedure (mean glandular dose, MGD) remains a concern in popular press even though the benefit of screening largely outweighs the risk of radiation-induced cancer [1]. Radiologists constantly try to reduce breast dose to the lowest amount technically achievable to alleviate the concern, in particular for women undergoing regular examinations in the age interval of systematic screening (40–74 years of age).

MGD estimation is done routinely as a part of quality control procedures [2]. Large variations of MGD have been reported in the literature depending on the technology and protocol used. For example, Bosmans et al. have reported a 60% higher breast dose delivered by computed radiography systems as compared to digital radiography systems [3]. At the same time as trying to reduce breast dose, radiologists strive for an increased image quality to reduce false positives/negatives in breast screening [4]. To address this issue, several novel techniques have been developed, including 3D imaging such as digital breast tomosynthesis (DBT) [5,6] and breast computed tomography (BCT) [7].

Currently, the standard method for breast cancer screening is digital x-ray mammography. It relies on the selective absorption of radiation by tissues of different density in the patient. Detection efficiency therefore depends on the composition of the breast tissue: detecting a lesion in a dense breast is much more difficult than in a breast composed mostly of adipose tissue. This poses a problem of diagnostic accuracy in the subgroup of women with dense breasts, which overlaps

* Corresponding author.
E-mail address: vincent.beaudoux@u-bordeaux.fr (V. Beaudoux).

https://doi.org/10.1016/j.ejmp.2019.03.026
Received 5 February 2019; Received in revised form 21 March 2019; Accepted 24 March 2019
Available online 28 March 2019

Fig. 1. DOSXYZnrc view of one of the DICOM images used for breast dose calculation with isodoses curves in relative dose.

significantly with the group of women of less than 50 years of age. The question has been raised whether photon absorption is the only physical process that can be exploited for the acquisition of diagnostic breast images. Several groups have advocated the use of phase contrast imaging as an alternative. Phase contrast 3D imaging would be of particular interest, as it could potentially maximize detection efficiency while providing patient comfort by removing the need for breast compression [8,9].

The challenge in constructing a novel mammography system consists in the reduction of breast dose while maintaining an image quality equivalent or superior to this of current techniques. In this context, the need of estimating MGD accurately is no longer restricted to the estimation of cancer-induction risk. It is also a pivotal parameter for the design and optimisation of the new mammography system.

Breast dose cannot be obtained with direct measurements of dose in patients. MDG estimation is instead largely based on the use of Monte Carlo calculated conversion factors that translate measurements of incident air kerma to breast dose [2]. While at the design phase of a novel mammography system based on phase-contrast imaging, it is important to conduct a detailed study of the dose dependence on several parameters. These include not only the geometrical specifications of the system, but also the method of primary photon generation and their energy spectrum, the image reconstruction algorithms and the implementation of clinical protocols. To this end, Monte Carlo calculations are an indispensable tool. Geant4 is a Monte Carlo code [10–12] that has been frequently used for mammography applications [13–15]. In this work, we validate the physics options of Geant4 v.10.4 with the intent of using the code for the design and optimisation of a mammography system based on phase contrast imaging (XPulse project). We have used EGSnrc [16] as a reference, as it is a Monte Carlo code broadly used in medical physics applications. We compared dose distributions calculated for various Geant4 physics implementations and various geometries with EGSnrc results. We performed comparisons of doses in homogeneous phantoms and in patient CT images. In addition, we utilized both Monte Carlo codes to study the dependence of breast dose on primary photon energy.

2. Materials and methods

We used the same geometry and primary particle definitions in both Geant4 and EGSnrc simulations. These are explained in Sections 2.1 and 2.2, respectively. Simulation parameters specific to Geant4 and to EGSnrc are addressed in Sections 2.3 and 2.4, respectively.

2.1. Geometry definition in the Monte Carlo simulations

We defined a phantom geometry as a cylinder of 7-cm radius and 10-cm length (referred to in the following as “phantom 1” for clarity). The cylinder was divided in depth into layers that could be filled with different materials. For the scoring of the longitudinal energy deposition, we placed along the axis of the 7-cm radius cylinder an inner cylinder of 0.5-cm radius. The inner cylinder was divided into 100 layers of 1 mm depth each, allowing the scoring of longitudinal energy depositions with a binning of 1 mm in all phantom simulations. The

inner and outer cylinders were always assigned the same material as a function of depth.

The materials used were water, beryllium, silver, lead, and lung, soft tissue and cortical bone [17]. The simulations of homogeneous phantoms were made for water, beryllium and silver. For the silver simulation we created a separate phantom (referred to in the following as "phantom 2") with the same cylinder radii as above but with a longitudinal division/binning of 0.1 mm over a total depth of 1 cm (100 bins). For the simulations of the inhomogeneous (layered) phantoms, we used the same cylinders with a total depth of 10 cm, and several divisions in depth for two different cases. In the first case ("phantom 3"), we used slabs of 2 cm of water, 2 cm of lung, 2 cm of water again, 3 cm of air and finally 1 cm of lead. In the second case ("phantom 4"), we used 5 layers of 2 cm each and the following order of materials: water, lung, cortical bone, water and (soft) tissue.

Finally, we used DICOM image of a patient treated for a breast cancer in our Institute to perform breast dose calculations (Fig. 1). Four materials were defined: air, lung, tissue and cortical bone (ICRU). The geometry of the DICOM images was constructed using DicomRegularDetectorConstruction() in the DICOM Geant4 example and the standalone dedicated program ctcreate in DOSXYZnrc.

2.2. Particle source

The same primary particle definition was used in both Monte Carlo codes. A monochromatic point beam of energy 20 keV, 60 keV and 100 keV was generated for the calculation of longitudinal energy depositions in phantoms. The beam was generated at the front face of the phantoms and its direction was along their main axis.

A square beam of 1 cm × 1 cm was implemented for the dose calculation in the DICOM images. Beam energy varied between 20 keV and 100 keV, with a 10-keV step. The beam was generated approximately at half length of the breast at the beginning of the DICOM image, as shown in Fig. 1. One hundred million primary particles were generated for all simulations and both Monte Carlo codes, as used in the phantom study reported in [18].

2.3. Geant4 simulations

Geant4 is a Monte Carlo code for the simulation of the passage of particles through matter. It is used in many high-energy physics experiments and in several application fields, such as astrophysics, radiation protection or medical physics. Its functionality and modelling capabilities in event category, tracking category, geometry module, electromagnetic physics and particle-matter interactions make it particularly interesting for simulating mammography systems.

Geant4 allows the user to choose among several models of electromagnetic low-energy physics. Geant4 also offers the possibility of creating complex geometry and particle source configurations, while maintaining the flexibility of its design.

For this study, simulations were performed with the 10.4 version of the toolkit (patch 02). We compared energy distributions in water and in phantoms of different materials calculated using the Livermore, Penelope and Standard (option 4) electromagnetic Physics Lists (PLs). In the energy range of 10 keV to 100 keV, option 4 includes the Auger effect while fluorescence is disabled. Livermore models are used for photoelectric, Rayleigh and Compton processes. Penelope models are used for gamma conversion and ionization processes. Bremsstrahlung is performed with the Seltzer-Berger model and multiple scattering for electrons is implemented with the Goudsmit-Sounderson model with "UseSafetyPlus" step limitation, RangeFactor = 0.2, and Mott corrections applied [19]. In all simulations, a production threshold of 10 μm was used for all particles.

2.4. EGSnrc simulations

EGSnrc is a Monte Carlo code, written in MORTRAN3 (an extension of Fortran language), mainly used for the simulation of the passage of photons and electrons through matter. EGSnrc is an improved version of EGS4 developed by the National Research Council Canada (NRCC) and the SLAC National Accelerator Laboratory. Indeed, the accuracy and precision for charged particle transport mechanics and atomic scattering cross section data were improved. It allows the calculation of energy deposition between 1 keV and 10 GeV in homogeneous materials [16]. In all EGSnrc phantom simulations, default parameters were chosen.

The calculation of dose deposition in DICOM image was performed using DOSXYZnrc, an EGSnrc based code for absorbed dose calculations in 3 dimensions. Firstly, we used the default parameters. We used the default PEGS4 file for the generation of material data. The global cut-off energy for electron and photon transport, respectively ECUT and PCUT, were set to 10 keV. The EXACT algorithm was used in order for particles to cross boundaries in a single scattering mode and the distance from a boundary at which this transition is made was 3 (default skin depth). PRESTA II was used as electron-step algorithm. The maximum fractional energy loss per step, ESTEPE was set to its default value: 25% of the kinetic energy of the particles. Finally, we performed dose calculations using the DICOM image and more accurate parameters. We produced a new PEGS4 file containing material data for an ECUT and PCUT set to 1 keV. Electronic stopping power and cross sections for simple element and ICRU materials were adapted for these new cut-offs. We also decreased the maximum fractional energy loss per step, ESTEPE, to 1%.

3. Results

We present the comparison of longitudinal energy distributions in water for different Geant4 Physics Lists in Section 3.1. Section 3.2 addresses the comparison of longitudinal energy distributions in phantoms of various materials between Geant4 and EGSnrc. Finally, we discuss the calculation of breast dose in DICOM images using both Monte Carlo codes in Section 3.3.

3.1. Geant4 physics list comparison

In the left column of Fig. 2, we compared longitudinal energy depositions calculated in water using the Standard Electromagnetic Physics List option 4 (lines) with results calculated using the Livermore Physics List (circles). Energy values were normalised to the number of primary photons (10^8 in all simulations) and depth (bin width of 1 mm). The right column shows the relative difference of energy deposits ((option 4 – Livermore)/option 4). The first row of plots refers to primary photons of 20 keV, the second row was calculated for primary photons of 60 keV and the last row shows results for a beam of 100 keV. Fig. 3 has the same disposition as Fig. 2, but it compares results for option 4 with the Penelope Physics List instead.

3.2. Comparison of longitudinal energy distributions between Geant4 and EGSnrc

Figs. 4 and 5 show results calculated using the geometry of phantom 1. Fig. 4 has the same disposition as Figs. 2 and 3 above. It presents longitudinal energy depositions scored in water with Geant4 option 4 (circles) and EGSnrc (solid line) for beam energies of 20 keV, 60 keV and 100 keV. Fig. 5 shows longitudinal energy distributions in phantom 1 for beryllium (circles show Geant4 results and lines show EGSnrc results) for a beam of 100 keV. In both figures, the binning of the horizontal axis is 1 mm.

The geometry of phantom 2 was used to calculate energy distributions as a function of depth in silver (Fig. 6) for a beam of 100 keV. The

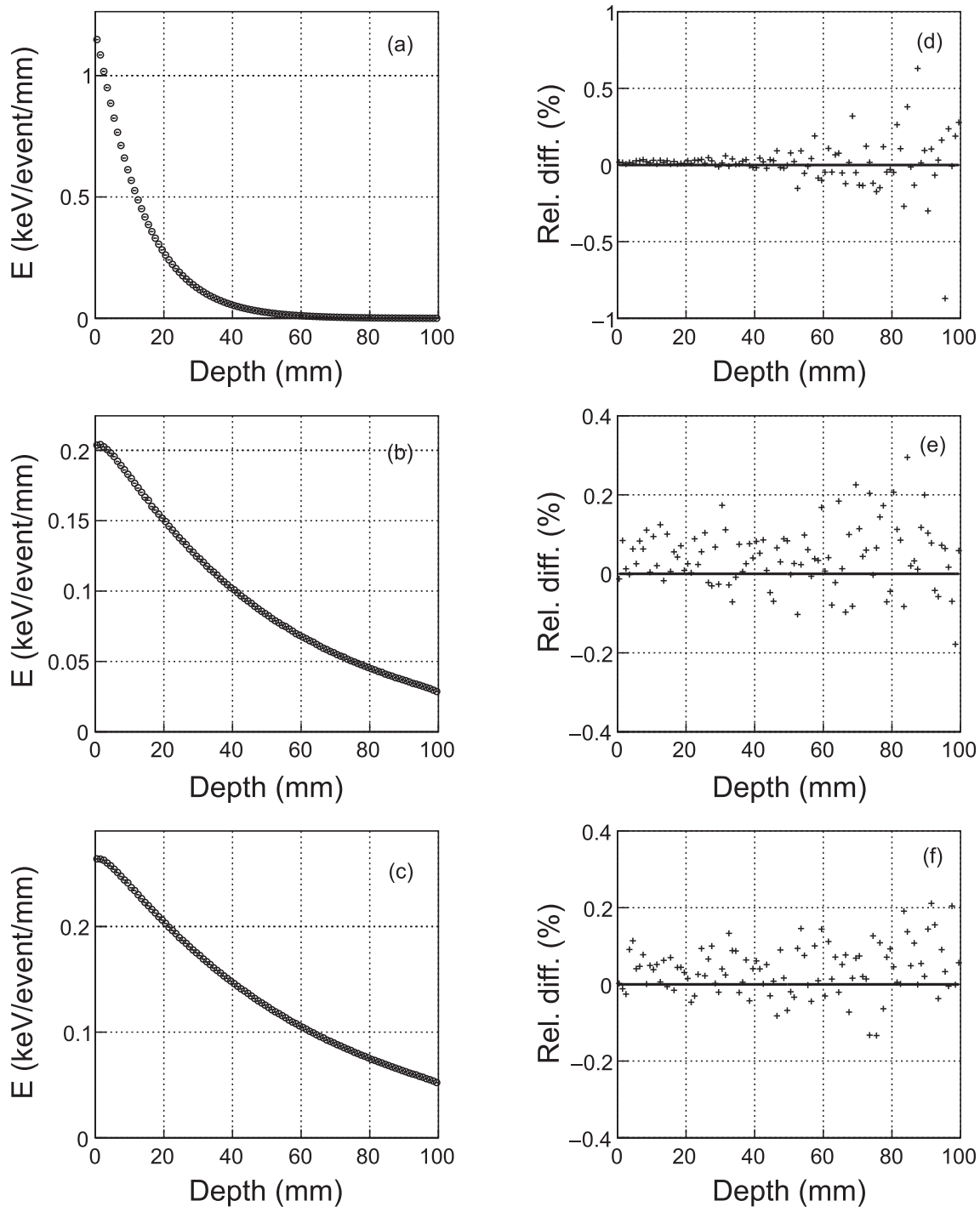

Fig. 2. Left column: Longitudinal energy distributions in water for beam energies of (a) 20 keV, (b) 60 keV, (c) 100 keV. Circles = Geant4 Livermore PL. Lines = Geant4 Standard Electromagnetic PL option 4. Right column: Relative differences of the energy depositions shown on the left (Livermore-Standard)/Standard.

circles show Geant4 calculations and the line shows EGSnrc calculations. The binning of the two plots is 0.1 mm in depth.

We used phantom 3 to calculate the energy deposits shown in Fig. 7. The disposition of the plots is the same as in Fig. 2. The vertical axes of Fig. 7d, e and f have been truncated for better visibility as explained in Section 4. The sequence of materials was water, lung, water, air and lead.

Finally, we present results obtained using the geometry of phantom 4 in Fig. 8. Again, we used the same disposition as in Fig. 2. The materials used were water, lung, cortical bone, water and (soft) tissue (ICRU 44 definitions).

3.3. Comparison of breast dose in DICOM images between Geant4 and EGSnrc

Fig. 9a shows absorbed dose scored in all voxels with the breast of the patient shown in Fig. 1 as a function of beam energy. Dose values were normalised to the number of primary photons (10^8). The squares show doses calculated using option 4 PL of Geant4. The circles show doses calculated with DOSXYZnrc. The doses shown in the figure

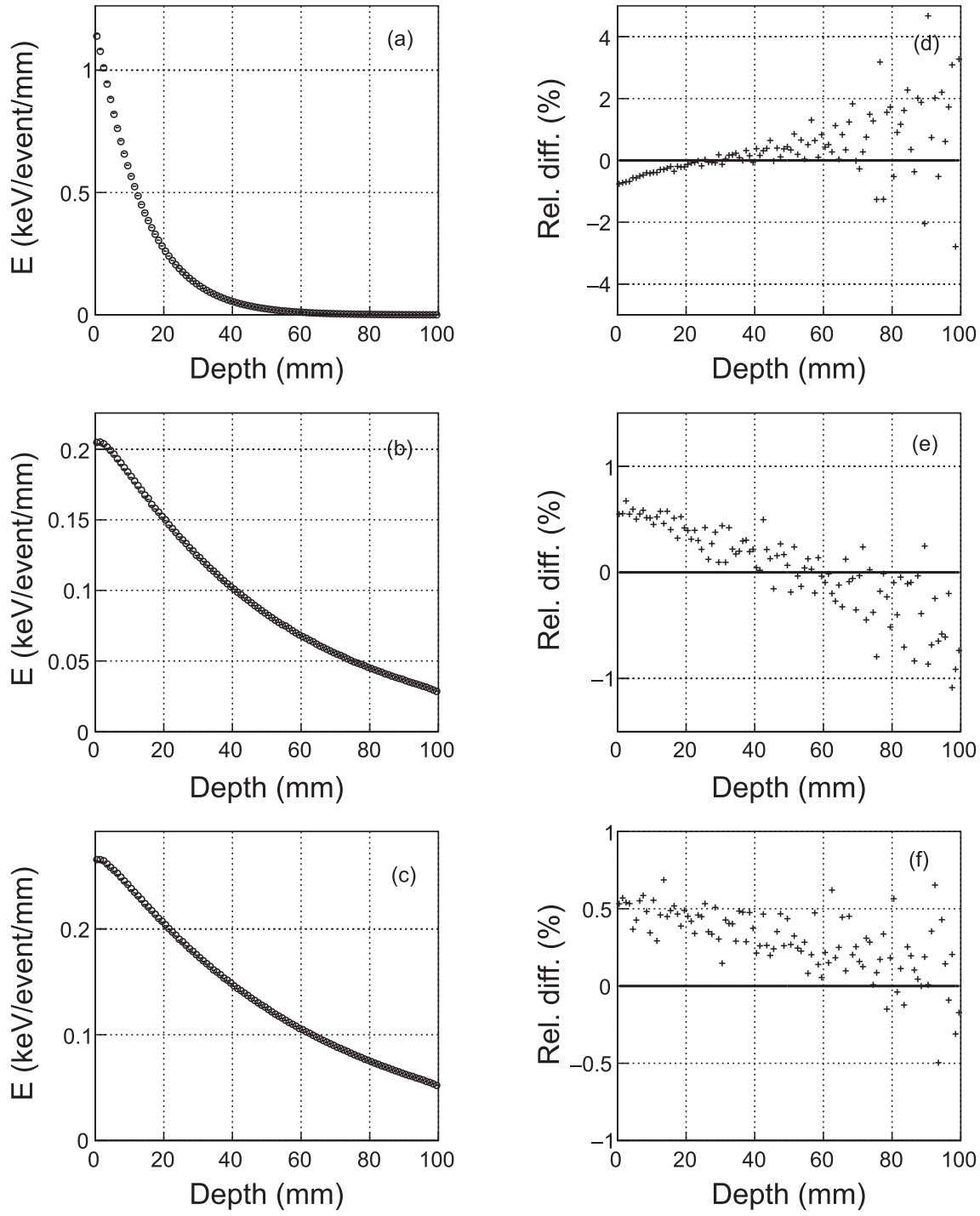

Fig. 3. Left column: Longitudinal energy distributions in water for beam energies of (a) 20 keV, (b) 60 keV, (c) 100 keV. Circles = Geant4 Penelope PL. Lines = Geant4 Standard Electromagnetic PL option 4. Right column: Relative differences of the energy depositions shown on the left (Penelope-Standard)/Standard.

represent the sum of doses scored in all voxels of the geometry where an energy deposit was made. Therefore, they do not correspond to the definition of MGD. Our intention was to evaluate their variation as a function of energy. Further calculations are needed, as discussed in Section 4. Fig. 9b shows the relative difference of the dose values presented in Fig. 9a ((Geant4-DOSXYZnrc)/DOSXYZnrc).

3.4. Comparison of execution times for Geant4 and EGSnrc

A comparison of the calculation times for the two Monte Carlo codes was made. Our calculation PC was composed of 48 processors Intel Xeon(R) CPU E5-2650 v4 − 2.20 GHz. Geant4 calculations were realized in multithreading mode. This was not the case for EGSnrc/DOSXYZnrc calculations, which were performed interactively.

For simulations performed using phantom 4 and for beam energy of 100 keV, the calculation time for Geant4 was 1 h 6 min (multithreading using 48 processors) whereas the calculation time for EGSnrc was 5 h 7 min (using 1 processor).

4. Discussion

The aim of this study was to compare the electromagnetic physics

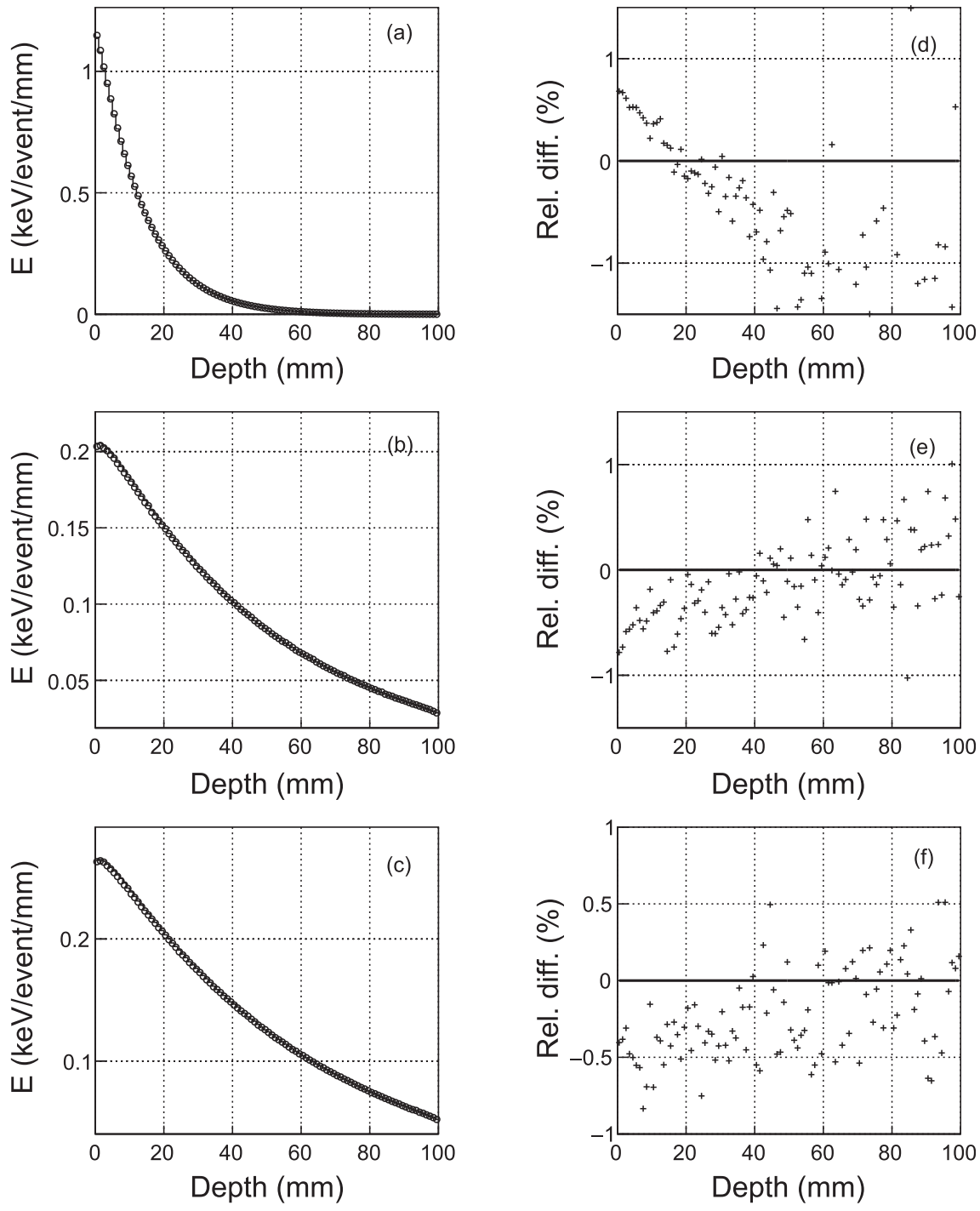

Fig. 4. Left column: Longitudinal energy distributions in water for beam energies of (a) 20 keV, (b) 60 keV, (c) 100 keV. Circles = Geant4 Standard Electromagnetic PL option 4. Line = EGSnrc. Right column: Relative differences of the energy depositions shown on the left (Geant4-EGSnrc)/EGSnrc.

options of Geant4 v10.4 and to validate them by using EGSnrc results as a reference. The primary particles were photons in an energy range that would be relevant for mammography imaging based on phase contrast (20–100 keV). We compared dose distributions in homogeneous phantoms and in DICOM images. We also addressed the question of breast dose dependence on beam energy.

Several Geant4 low-energy studies have utilized the Standard Electromagnetic (EM) Physics List (PL) option 4, as this physics list provides the most detailed implementation of electromagnetic processes for low energy photons and it was suggested by the AAPM TG-195 [20]. Other options in the Standard Electromagnetic Physics List series are meant for fast simulation or high energy applications. However, we were interested to compare the performance of Standard EM PL option 4 with Physics Lists maintained by the Low Energy Electromagnetic Physics Group, namely Penelope and Livermore, as these have also been used in mammography simulations. We simulated longitudinal energy depositions in water for beam energies in the interval 20–100 keV with steps of 10 keV. As the results showed similar agreement for all energies, we presented results only for energies of 20 keV, 60 keV and 100 keV. As shown in Fig. 2, the agreement between option 4 and Livermore PLs is within 0.5% for all energies and all depths in water, except for the 20 keV beam and for depths larger than 6 cm,

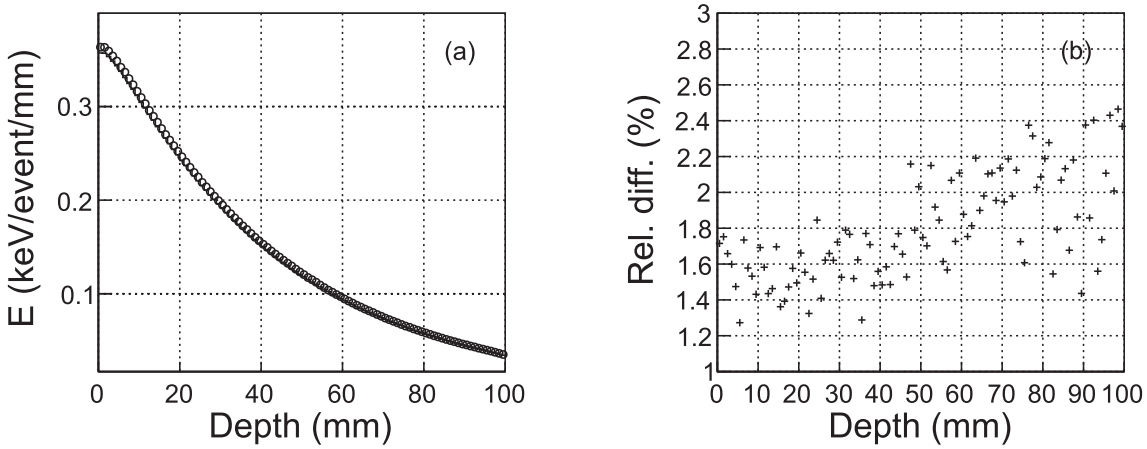

Fig. 5. (a) Longitudinal energy distributions in Be for beam energy of 100 keV. Circles = Geant4 Standard Electromagnetic PL option 4. Line = EGSnrc. (b) Relative differences of the energy depositions shown on the left (Geant4-EGSnrc)/EGSnrc.

where the energy depositions are negligible. Livermore has a slight tendency to calculate higher energy deposits for 60 keV and 100 keV but overall, relative energy differences are well centered around zero (Fig. 2e and f). We concluded that option 4 and Livermore Physics Lists can be used interchangeably for mammography simulations, as found in the literature. For example, Livermore PL was used in [21] and [22], whereas [18] and [20] have used option 4.

We found more important differences in energy depositions in water between option 4 and Penelope PLs (Fig. 3). For all energies, relative differences seem to have a linear tendency, which is increasing as a function of depth at 20 keV (Fig. 3d) or decreasing as a function of depth at higher energies (Fig. 3e and f). Relative energy deposition differences for a 20 keV beam are as large as 2% for depths less than 6 cm (to compare with 0.5% in the case of Livermore PL). Relative differences for 60 keV and 100 keV photons are within 1% (Fig. 3e and f). This would suggest that Penelope PL may not be a good candidate for very low energy photons.

Fig. 4 shows an agreement within 1.5% between longitudinal energy depositions calculated in water with Geant4 option 4 and EGSnrc. There seems to be a linear tendency in the relative energy differences between the two codes, which becomes more pronounced as the beam energy decreases (Fig. 3d). We found the agreement between Geant4 and EGSnrc in water to be acceptable. As this was found best at 100 keV (1%), we simulated energy depositions for photons of that energy in heavier materials to investigate if the level of agreement is maintained for high Z values. Figs. 5 and 6 suggest that the discrepancies between the two codes become more important as Z increases, reaching 3% for Be (Fig. 5b) and 8% for Ag (Fig. 6b). We concluded that further investigations are needed in order to validate our physics list for use with heavier elements. We would like to note that in EGSnrc energy deposition at a step is computed in average, in Geant4 sampling of energy loss fluctuation is performed. The difference in tails of radiation dose distribution may be explained in part by this principal difference between two simulations. This difference should be more pronounced for large Z.

Variations of energy deposition at interfaces of varying density were also relevant in the context of our study. Figs. 7 and 8 show the comparison of longitudinal energy depositions calculated with option 4 and EGSnrc in phantoms consisting of homogeneous layers of different materials. Fig. 7d, e and f have the vertical axis truncated at 5% to make the plots readable but larger deviations were observed. The largest discrepancies we found in air were 30% at 20 keV, 12% at 60 keV and 8% at 100 keV. We believe that we need to repeat these simulations with higher statistics before we can evaluate these discrepancies. However, we do not expect a great improvement in the comparison at higher statistics as the dose deposition in air is relatively low. The deviations in Pb are not visible for 20 keV because the photons are absorbed immediately as they enter this layer. For beams of 60 and 100 keV, we observed relative dose differences up to 600% and 100%, respectively, between the two codes. Further investigation is needed with a thin-layer phantom in this case. Relative differences within the water-lung-water layers where within 1.5% for all energies (Fig. 7d, e,

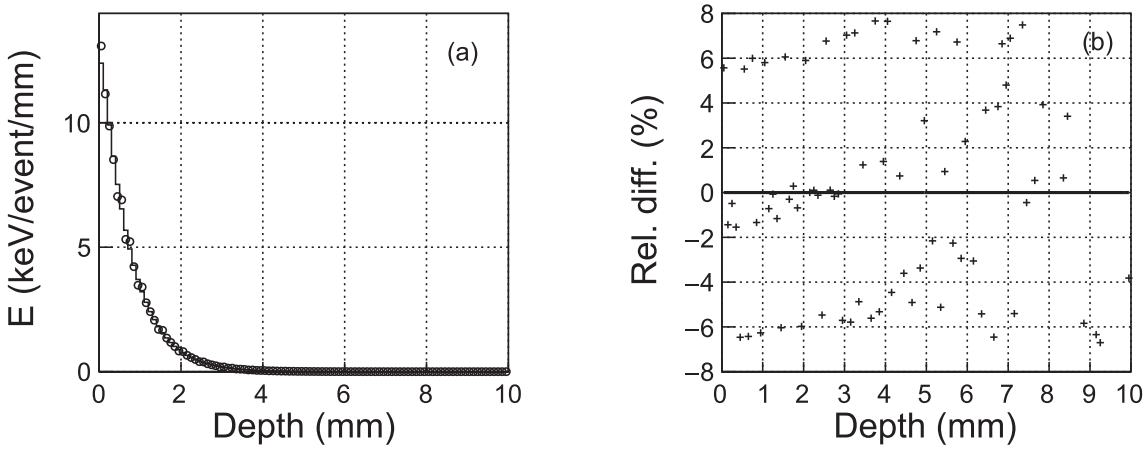

Fig. 6. (a) Longitudinal energy distributions in Ag for beam energy of 100 keV. Circles = Geant4 Standard Electromagnetic PL option 4. Line = EGSnrc. (b) Relative differences of the energy depositions shown on the left (Geant4-EGSnrc)/EGSnrc.

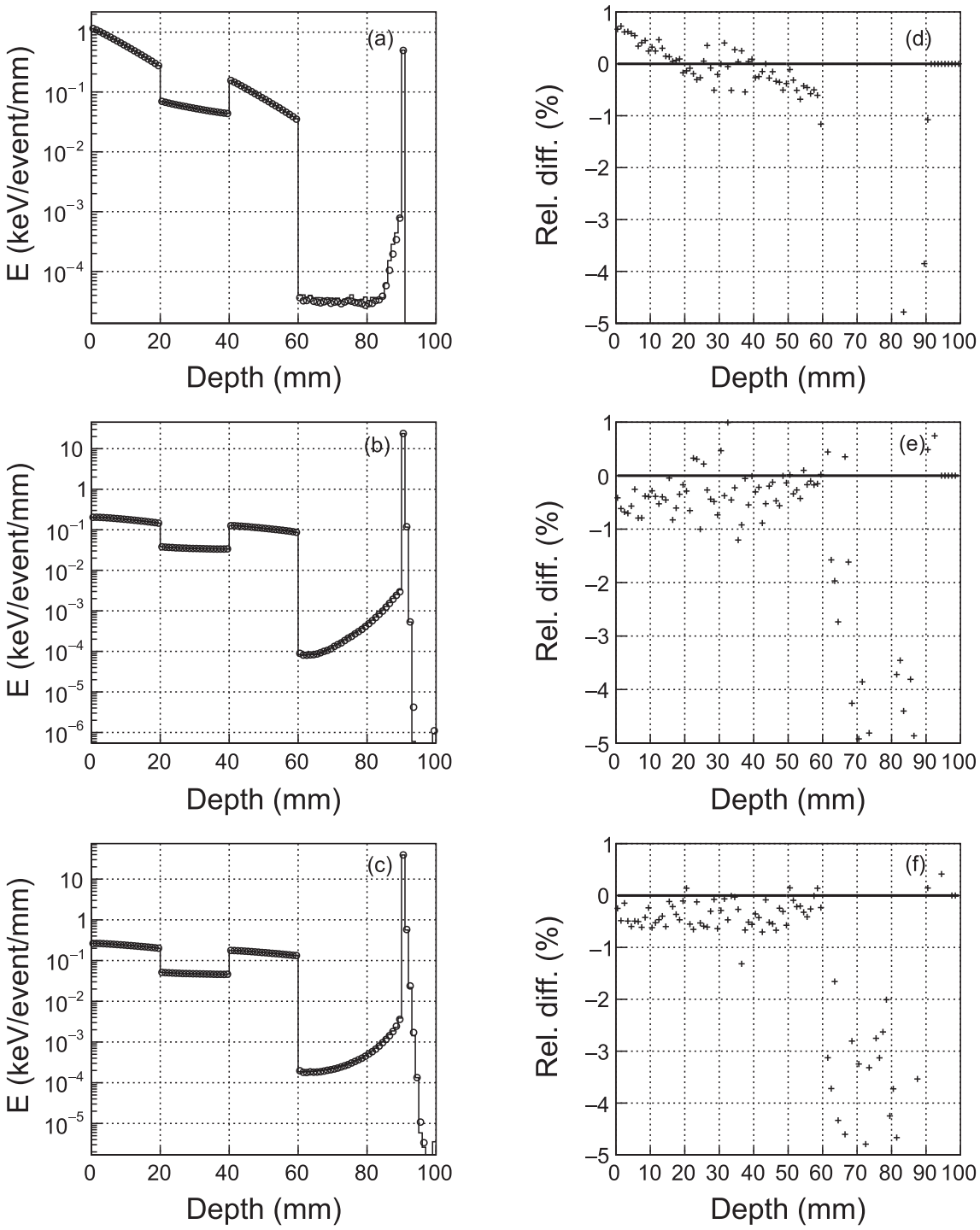

Fig. 7. Left column: Longitudinal energy distributions in a layered phantom consisting of 2 cm water, 2 cm lung, 2 cm water, 3 cm air and 1 cm lead for beam energies of (a) 20 keV, (b) 60 keV, (c) 100 keV. Circles = Geant4 Standard Electromagnetic PL option 4. Line = EGSnrc. Right column: Relative differences of the energy depositions shown on the left (Geant4-EGSnrc)/EGSnrc.

f). We find this result to be acceptable. In Fig. 8d, the largest difference between Geant4 and EGSnrc was 50% in cortical bone, but the energy is too low to allow for an evaluation of this result. Relative dose differences in cortical bone were at most 3% at 60 keV (Fig. 8e) and 1% at 100 keV (Fig. 8f). We conclude that Geant4 and EGSnrc are in overall good agreement in biological tissues for photon energies between 20 keV and 100 keV.

Finally, we compare the dependence of breast dose on beam energy between the two codes (Fig. 9). We note that Fig. 9 shows dose deposited in all voxels within the breast volume, without differentiating between glandular tissue and adipose. A more detailed comparison needs to be made to take this into account. We observed acceptable differences (up to 6%) between Geant4 and EGSnrc for energies above 40 keV. Discrepancies up to 15% were found for lower energies. We do not have an explanation for this observation as of yet, further investigation is needed. It is worth noting, however, that both codes find a minimum of energy deposition around 60 keV. This is in agreement with previous studies [23]. More patient images will be used in the future to further evaluate the dose dependence on beam energy for different patient morphologies.

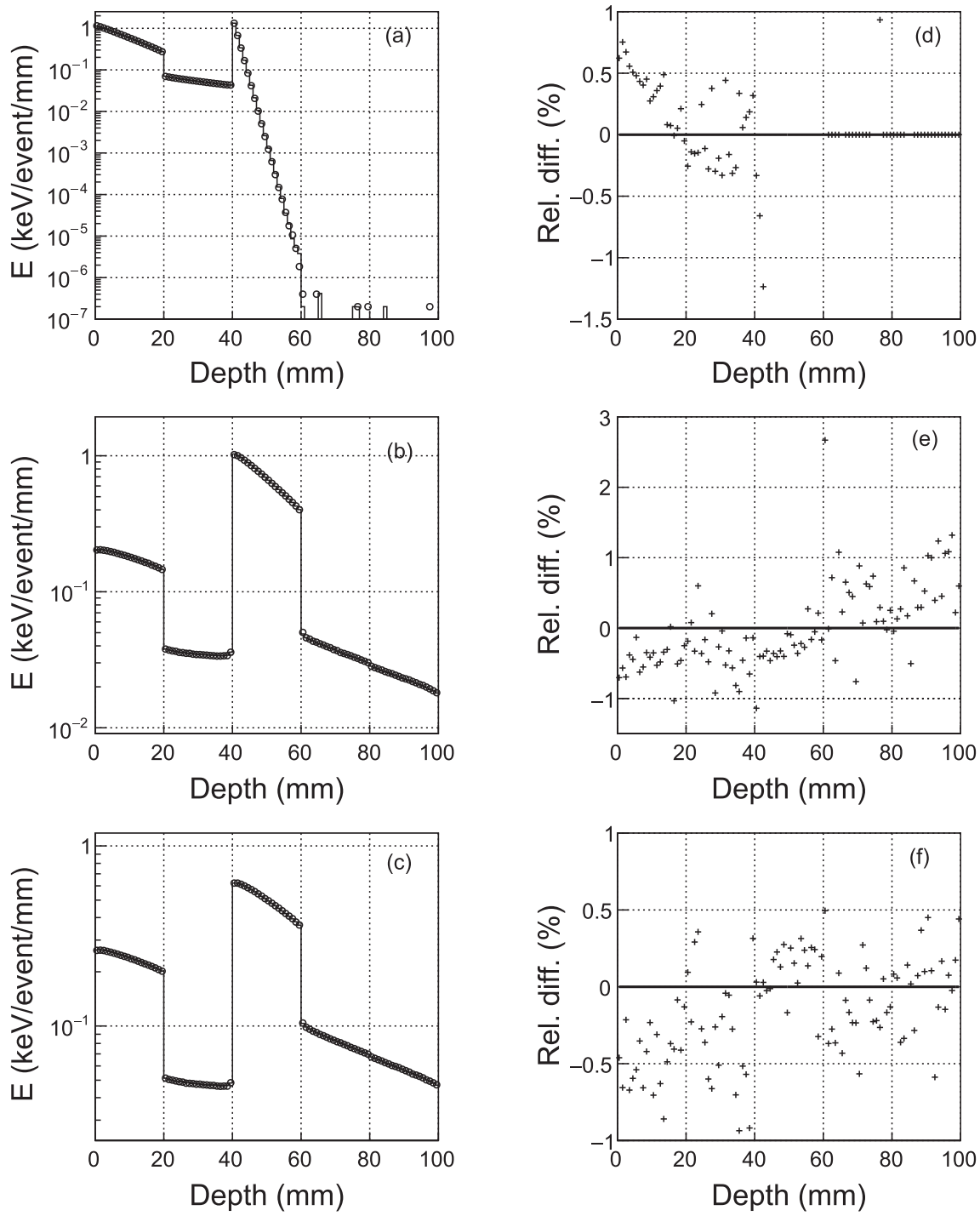

Fig. 8. Left column: Longitudinal energy distributions in a layered phantom consisting of 2 cm water, 2 cm lung, 2 cm cortical bone, 2 cm water and 2 cm soft tissue for beam energies of (a) 20 keV, (b) 60 keV, (c) 100 keV. Circles = Geant4 Standard Electromagnetic PL option 4. Line = EGSnrc. Right column: Relative differences of the energy depositions shown on the left (Geant4-EGSnrc)/EGSnrc.

Further simulations will be performed to compare Geant4 option 4 with EGSnrc in the case of thin layers of heavy materials that may be relevant in the construction of the prototype of our mammography system. In addition, further dose calculations need to be performed in patient DICOM images in order to obtain a more precise estimation of breast dose, and more notably, one that conforms better to the definition of MGD. A further shortcoming of this study is the use of monochromatic beams. A comparison between Geant4 and EGSnrc needs to be conducted for a more realistic energy spectrum, in particular to address discrepancies at lower photon energies, as the contribution of dose from bremsstrahlung photons may be an issue at high primary photon energies.

Finally, we note that our evaluation of execution times for a single phantom geometry (phantom 4) and beam energy of 100 keV indicated that EGSnrc is about 10 times faster than Geant4 if option 4 PL is used. A more thorough evaluation would be required to include more geometries and beam energies in order to better assess the performance of the two codes.

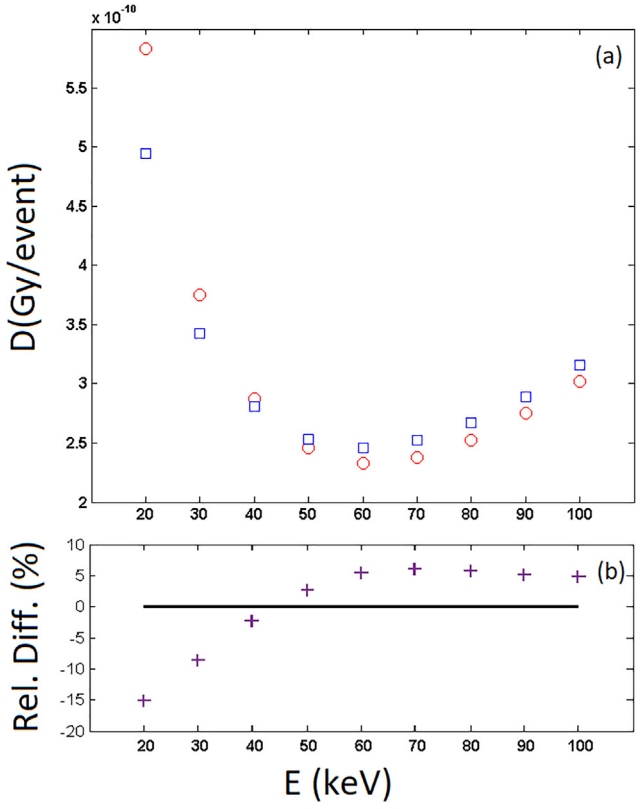

Fig. 9. (a) Dose (Gy/event) calculated with Geant4 Standard Electromagnetic PL option 4 (squares) and DOSXYZnrc (circles) in the geometry shown in Fig. 1. (b) Relative difference of the doses shown in (a), (Geant4-EGSnrc)/EGSnrc.

5. Conclusions

We found an overall good agreement between Geant4 and EGSnrc for energy depositions in water and biological materials such as soft tissue, lung and bone. More investigations are needed to evaluate discrepancies observed in heavier materials, such as beryllium, silver and lead. Comparison of breast dose depositions in DICOM images showed the same trend as a function of primary photon energy in the two codes, confirming an optimal beam energy for mammography screening around 60 keV.

Acknowledgements

This work was done as part of the XPulse project funded by the Nouvelle-Aquitaine regional council – France and by the European Development Fund (FEDER).

References

[1] Yaffe MJ, Mainprize JG. Risk of radiation-induced breast cancer from mammographic screening. Radiology 2011;258(1):98–105.
[2] Dance DR, Sechopoulos I. Dosimetry in x-ray-based breast imaging. Phys Med Biol 2016;61(19):R271–304.
[3] Bosmans H, De Hauwere A, Lemmens K, Zanca F, Thierens H, Van Ongeval C, et al. Technical and clinical breast cancer screening performance indicators for computed radiography versus direct digital radiography. Eur Radiol 2013;23:2891–8.
[4] Yaffe MJ, Bloomquist AK, Hunter DM, Mawdsley GE, Chiarelli AM, Muradali D, et al. Comparative performance of modern digital mammography systems in a large breast screening program. Phys Med 2013;40(12):121915–25.
[5] Sechopoulos I. A review of breast tomosynthesis. Part I. The image acquisition process. Phys Med 2013;40(1):014301.
[6] Sechopoulos I. A review of breast tomosynthesis. Part II. Image reconstruction, processing and analysis, and advanced applications. Phys Med 2013;40(1):014302.
[7] Sarno A, Mettivier G, Russo P. Dedicated breast computed tomography: basic aspects. Phys Med 2015;42(6):2786.
[8] Li K, Ge Y, Garrett J, Bevins N, Zambelli J, Chen GH. Grating-based phase contrast tomosynthesis imaging: proof-of-concept experimental studies. Phys Med 2014;41(1):011903.
[9] Szafraniec MB, Millard TP, Ignatyev K, Speller RD, Olivo A. Proof-of-concept demonstration of edge-illumination x-ray phase contrast imaging combined with tomosynthesis. Phys Med Biol 2014;59:N1–10.
[10] Allison J, et al. Geant4 developments and applications. IEEE Trans Nucl Sci 2006;53(1):270–8. https://doi.org/10.1109/tns.2006.869826.
[11] Agostinelli S, et al. Geant4 – a simulation toolkit. Nucl Instrum Meth Phys Res 2003;A506:250–303. https://doi.org/10.1016/S0168-9002(03)01368-8.
[12] Allison J, et al. Recent developments in Geant4. Nucl Instrum Meth 2016;A835:186–225.
[13] Sechopoulos I, Suryanarayanan S, Vedantham S, D'Orsi C, Karellas A. Computation of the glandular radiation dose in digital tomosynthesis of the breast. Phys Med 2007;34(1):221–32.
[14] Sechopoulos I, D'Orsi C. Glandular radiation dose in tomosynthesis of the breast using tungsten targets. J Appl Clin. Med Phys 2008;9(4):161–71.
[15] Sechopoulos I, Bliznakova K, Qin X, Fei B, Feng SSJ. Characterization of the homogeneous tissue mixture approximation in breast imaging dosimetry. Phys Med 2012;39:5050–9.
[16] Rogers DWO, Kawrakow I, Seuntjens JP, Walters BRB, Mainegra-Hing E. NRC user codes for EGSnrc. Technical Report PIRS-702(RevB). Ottawa, Canada: National Research Council of Canada; 2003.
[17] ICRU. Tissue substitutes in radiation dosimetry and measurement. ICRU Report 44. 1989.
[18] Fedon C, Caballo M, Sechopoulos I. Internal breast dosimetry in mammography: Monte Carlo validation in homogeneous and anthropomorphic breast phantoms with a clinical mammography system. Med Phys 2018;45(8):3950–61.
[19] Incerti S, Ivanchenko V, Novak M. Recent progress of Geant4 electromagnetic physics for calorimeter simulation. JINST 2018;13:C02054.
[20] Sarno A, Mettivier G, Di Lillo F, Russo P. A Monte Carlo study of monoenergetic and polyenergetic normalized glandular dose (DgN) coefficients in mammography. Phys Med Biol 2017;62:306–25.
[21] Mettivier G, Fedon C, Di Lillo F, Longo R, Sarno A, Tromba G, et al. Glandular dose in breast computed tomography with synchrotron radiation. Phys Med Biol 2016;61:569–87.
[22] Fedon C, Longo F, Mettivier G, Longo R. GEANT4 for breast dosimetry: parameters optimization study. Phys Med Biol 2015;60:N311–23.
[23] Krejci F, Jakubek J, Kroupa M. Hard x-ray phase contrast imaging using single absorption grating and hybrid semiconductor pixel detector. Rev Sci Instrum 2010;81:113702.